Styrene maleic acid anhydride copolymer (SMA) for the encapsulation of sparingly water-soluble drugs in nanoparticles

S. Yamamoto[1], Y. Kaneo[1*], H. Maeda[2]

[1]Laboratory of Biopharmaceutics, Faculty of Pharmacy and Pharmaceutical Sciences,
Fukuyama University, Fukuyama, Hiroshima, 729-0292, Japan
[2]Laboratory of Microbiology and Oncology, Faculty of Pharmaceutical Sciences, Sojo University, Kumamoto, 860-0082, Japan
*Correspondence: kaneo@fupharm.fukuyama-u.ac.jp

Styrene maleic acid copolymer (SMA) is widely used in various industrial applications, such as adhesives and coatings, because of its good durability and low cost. In this study, we investigated the biological safety and functions of nanoparticle formulations with varying molecular weights of SMA. The toxicity of SMA, measured by hemolytic activity and body weight loss, was examined in mice. Amphotericin B (AmB) and all-trans retinoic acid (ATRA) are limited in clinical use because of their poor water solubility. We prepared AmB- and ATRA-loaded SMA nanoparticles for the first time; these are self-assembled nanoparticles with a high drug-loading capacity. The formation of monodispersed nanoparticles by self-assembly of SMA and their complex formations with drugs were studied by size-exclusion chromatography (HPSEC) and dynamic light scattering. After intravenous injection of the drug-loaded SMA nanoparticles, prolonged blood circulation of AmB and ATRA was observed.

Key words: Styrene maleic acid anhydride copolymer – SMA – Nanoparticle – Critical aggregation concentration – Amphotericin B – All-trans retinoic acid – Biodistribution.

Styrene maleic acid anhydride copolymer (SMA) is an alternating copolymer that is easily formed by free radical copolymerization of maleic anhydride and styrene. SMA can be modified by reacting the functional anhydride groups with different nucleophiles. SMA is widely used in various industrial applications, such as in adhesives and coatings, because of its good durability and low cost. It has no teratogenic, acute, or chronic toxic effects [1].

In 1979, Maeda *et al.* reported the first synthesis of the anticancer protein neocarzinostatin (NCS) conjugated to SMA, which they named SMANCS. Later studies found that SMANCS accumulates in tumor tissues to a greater extent than NCS [2,3]. These studies reported that a micellar formulation of pirarubicin using SMA exhibited an excellent tumor targeting capacity due to the enhanced permeability and retention (EPR) effect. The SMA-pirarubicin micelles contributed to prolonged survival *in vivo* in a murine liver metastasis model [4,5]. An antitumor compound, zinc protoporphyrin IX (ZnPP)-SMA micelles, also showed remarkable cytotoxicity against a variety of tumor cells. It demonstrated antitumor effects in Meth A fibrosarcoma and B16 melanoma tumor-bearing mice [6,7].

Amphotericin is an antifungal agent; it was isolated in 1956 from a soil actinomycete, streptomyces nodosus and exists in two forms, A and B. The latter, amphotericin B (AmB), is more active and is used primarily as a broad-spectrum, fungicidal antibiotic in the treatment of life-threatening systemic fungal infections [8,9]. For many years, the classic Fungizone (AmB-desoxycholate) was the mainstay of antifungal therapy; however, AmB treatment is frequently associated with numerous toxicities, especially nephrotoxicity and infusion-related adverse effects, that limit its use [10, 11].

The strong lipophilic properties of AmB inspired attempts to encapsulate it in liposomes and to investigate its binding with lipid complexes in an effort to increase both its efficacy and safety. Subsequently, three lipid formulations, Amphotec (AmB colloidal dispersion), Abelcet (AmB lipid complex), and AmBisome (liposomal AmB), were developed and licensed [12-14]. These products are available; however, they are associated with some toxicity and thus are not universally effective. Therefore, alternative formulations need to be developed.

All-trans retinoic acid (ATRA) is a physiologically active form of a metabolic product of vitamin A. ATRA has been shown to act as an anticancer agent in a variety of cancers such as acute promyelocytic leukemia, Kaposi's sarcoma, head and neck squamous cell carcinoma, and neuroblastoma.

Vesanoid is an oral preparation of ATRA that is used to treat acute promyelocytic leukemia. However, the oral absorption of ATRA is highly variable [15]. Other routes of administration have been investigated to enhance the therapeutic efficacy of ATRA. Among them, parenteral formulations seem to be a good alternative for ATRA administration; these formulations reliably increase the potency and duration of ATRA's activity in cancer patients. The poor water solubility of ATRA, however, has been a limiting factor in its clinical use.

One of the approaches for improving a drug's performance and reducing its toxicity involves the use of a macromolecular carrier system [16]. Polymeric nanoparticles have been somewhat successful in delivering sparingly water-soluble drugs into systemic circulation [17-19].

In this study, SMA was selected as a vehicle because of its hydrophilic carboxyl groups and hydrophobic styrene rings. Because AmB and ATRA are sparingly soluble in water, we attempted to render them soluble by encapsulating them in amphiphilic SMA nanoparticles that we prepared, as encapsulation should enable AmB and ATRA to be effectively transported via the circulation.

I. MATERIALS AND METHODS
1. Materials

Butyl SMA (MW = 1,000) (But-SMA (1 k)) and SMA (MW = 1,000) (SMA (1 k)) were supplied by Kuraray (Kurashiki, Japan). The degree of butylation of But-SMA (1 k) was approximately 60 %. SMA (MW = 7,000) (SMA (7 k)) and SMA (MW = 10,000) (SMA (10 k)) were obtained from Wako Pure Chemical Industries, Ltd. (Osaka, Japan). All SMAs in the maleic anhydride form. AmB was obtained from Sigma-Aldrich Co., Ltd. (St. Louis, MO, United States). ATRA was obtained from Tokyo Chemical Industry Co., Ltd. (Tokyo, Japan).

J. DRUG DEL. SCI. TECH., 23 (3) 231-237 2013

Styrene maleic acid anhydride copolymer (SMA) for the encapsulation of sparingly water-soluble drugs in nanoparticles
S. Yamamoto, Y. Kaneo, H. Maeda

Fungizone was purchased from Bristol-Myers Squibb Co.,Ltd.(Tokyo, Japan). All other chemicals and reagents were of the highest grade commercially available.

2. Animals

Male ddY mice aged 5 weeks were purchased from Shimizu Laboratory Supplies (Shizuoka, Japan), housed under standard conditions, and given commercial food and tap water. All animal experiments were conducted in accordance with the institutional guideline for the care and use of laboratory animals for research, which also conforms to guidelines provided by the Science Council of Japan.

3. Preparation of amphiphilic styrene maleic acid copolymer and SMA nanoparticles

Each anhydride SMA (500 mg) was hydrolyzed in 10 mL of water adjusted to a pH of 13.5 with 1 M NaOH; anhydride SMAs were kept at 60 °C for a week. During this step, each anhydride SMA suspension became a clear solution; the pH was then adjusted back to 7.0 by the addition of 1 M HCl. Each SMA solution was dialyzed against distilled water for 72 h using a dialysis tube with a 100-500 Da cut-off. The distilled water was exchanged every 4 h. After dialysis, the sample solution in the tube was lyophilized.

The loading of sparingly water-soluble drugs was conducted using the hydrolyzed SMA solutions. AmB (10 mg) or ATRA (10 mg) was dissolved in 0.1 mL of dimethyl sulfoxide (DMSO). The drug solution was added to But-SMA (1 k), SMA (1 k), SMA (7 k) or SMA (10 k) solution; the amount used was equivalent to 50 mg of SMA in each case. The purification of each mixture solution was conducted using ultrafiltration (Amicon Ultra-15; cut-off molecular size 10 kDa, Millipore, United States). Each mixture was washed with distilled water five times by ultrafiltration, each time with a 5-fold greater volume of water than the solution (1 mL). The final solution was then lyophilized [20, 21].

4. Dynamic light scattering measurements

A Zetasizer Nano ZS, (Malvern Instrument, United Kingdom) equipped with a 4.0 mW, He-Ne laser (633 nm), was used to measure the dynamic light scattering (DLS) of the aqueous polymer solutions at 1 mg/mL and 25 °C. The scattering angle was fixed at 173 °. The particle diameters were taken from three 3-min runs for a total accumulation correlation function (ACF) time of 9 min. The zeta potentials of the nanoparticles were determined as follows: approximately 750 μL of each sample solution was placed in a disposable capillary zeta potential cell, and the measurement was performed at 25 °C.

5. Critical aggregation concentration measurements

The critical aggregation concentration (CAC) of the SMAs was determined by fluorescence spectroscopy (HITACHI 650-10S, Japan) with N-phenyl-1-naphthylamine (PNA) as the hydrophobic probe [22]. A known amount of PNA in acetone was added to each of a series of 10 mL vials, and the acetone was evaporated. Then, 2-mL aliquots of the SMA solution at concentrations ranging from 1.8 to 4,000 μg/mL were added to the vial; the final concentration of PNA was maintained at 1×10^{-7} M. The sample solutions were incubated at 40 °C for 1 h to incorporate PNA into the nanoparticles and were then left to cool at room temperature. The fluorescence emission spectra were scanned over wavelengths ranging from 350 to 600 nm at an excitation wavelength of 340 nm.

6. Hemolytic activity of SMAs [23, 24]

Blood from the vena cava of male ddY mice was collected and centrifuged at 2,000 rpm. Sheep blood was obtained from Nippon Biotest Laboratories Inc. (Tokyo, Japan) and treated by the same manner. The supernatant and buffy coat were pipetted, and the red blood cells

(RBCs) were diluted with an isotonic phosphate buffer at pH 7.4. The RBCs were lysed by adding water and the proper dilution factor was estimated from the UV absorbance of hemoglobin in the supernatant at 576 nm. A properly diluted sample of RBCs gave an absorbance of 0.4-0.5. Solutions of diluted RBCs with different concentrations of SMA were incubated at 37 °C for 30 min and then placed on ice to arrest hemolysis. The unlysed RBCs were immediately removed by centrifugation at 10,000 rpm for 30 s. The supernatant was collected and analyzed for hemoglobin with a UV spectrometer at 576 nm. The percentage of hemolyzed RBCs was determined using the following equation: % hemolysis = (Abs-Abs0)/(Abs100-Abs0) × 100, where Abs, Abs0, and Abs100 are the absorbance values for the sample, the negative control containing no hemolysis, and the 100 % lysed sample, respectively. The same procedure was adopted for both mouse and sheep RBCs.

7. Toxicity assay of SMAs

The toxicities of the SMAs were determined in groups of mice after intravenous administration of But-SMA (1 k), SMA (1 k), SMA (7 k), or SMA (10 k) at 20 mg/kg. A 5 % glucose solution served as the control. The mice were monitored daily for changes in weight over a two-week span.

8. HPSEC analysis

High-performance size exclusion chromatography (HPSEC) was carried out using a liquid chromatography apparatus (LC-9A, Shimadzu, Japan) equipped with a differential refractometer (RI-8000, Tosoh, Japan). A 7.8 × 300 mm TSK gel G4000PWXL column (Tosoh, Japan) was used at 40 °C. The mobile phase was water, with a flow rate of 1.0 mL/min. The injection volume was 50 µL. A three-dimensional analysis was also carried out using the HPSEC system equipped with a photodiode array detector (Waters, United States).

9. HPLC analysis

Chromatography was carried out using an HPLC system (LC-10AD, Shimadzu, Kyoto, Japan) equipped with a variable-wavelength UV detector (SPD-20A, Shimadzu, Kyoto, Japan). The detection wavelength of AmB was 405 nm and that of ATRA was 340 nm. A 4.6 × 150 mm C18 reversed phase column (TSKgel ODS 80TM, Tosoh, Tokyo, Japan) was used at ambient temperature. The mobile phase for AmB was a mixture of sodium acetate buffer (10 mM, pH 7.0) and acetonitrile (60:40 (v/v)); the mobile phase for ATRA was a mixture of methanol and 50 mM ammonium dihydrogenphoshate in water (90.5:9.5 (v/v)). The flow rate was 1.0 mL/min in both cases. The injection volume was 20 µL [25, 26].

10. Animal experiments

Male ddY mice were injected through the tail vein with drug-loaded SMAs at a dose of 2 mg/kg AmB or ATRA in 0.2 mL of 5 % glucose solution. At appropriate time points, mice were anesthetized and blood was collected from the vena cava. Organs, such as the liver, kidney, lungs, and spleen, were then excised and weighed. The blood was centrifuged at 10,000 rpm for 30 s, and the plasma was harvested. These samples were homogenized separately in methanol. Then, methanol was added to each homogenate to achieve a total volume of 10 mL. The samples were left for 1 h at room temperature before centrifuging at 3,000 rpm for 5 min. Eight milliliters of the supernatant of each sample was removed using a pipette and evaporated at 40 °C. The residue was dissolved in 400 μL of the mobile phase, which was passed through a membrane filter (0.45 μm) and injected into the HPLC system. The same extraction procedure was adopted for both AmB and ATRA.

The significance of the *in vivo* data was evaluated using Student's t-test. When the p value is less than 0.05, the difference was considered to be significant.

Styrene maleic acid anhydride copolymer (SMA) for the encapsulation of sparingly water-soluble drugs in nanoparticles
S. Yamamoto, Y. Kaneo, H. Maeda

J. DRUG DEL. SCI. TECH., 23 (3) 231-237 2013

II. RESULTS AND DISCUSSION
1. Critical aggregation concentration of SMA

The anhydride form of SMA is insoluble in water; the maleic anhydride residue of the SMA was then hydrolyzed to the water-soluble maleic acid form by adding NaOH (*Figure 1*). The lyophilized powder of the sodium salt of SMA was extremely water soluble.

The SMAs formed nanoparticles in an aqueous environment because of the aggregation of hydrophobic styrene groups. The critical
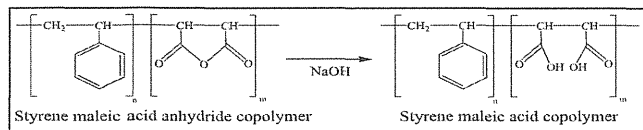
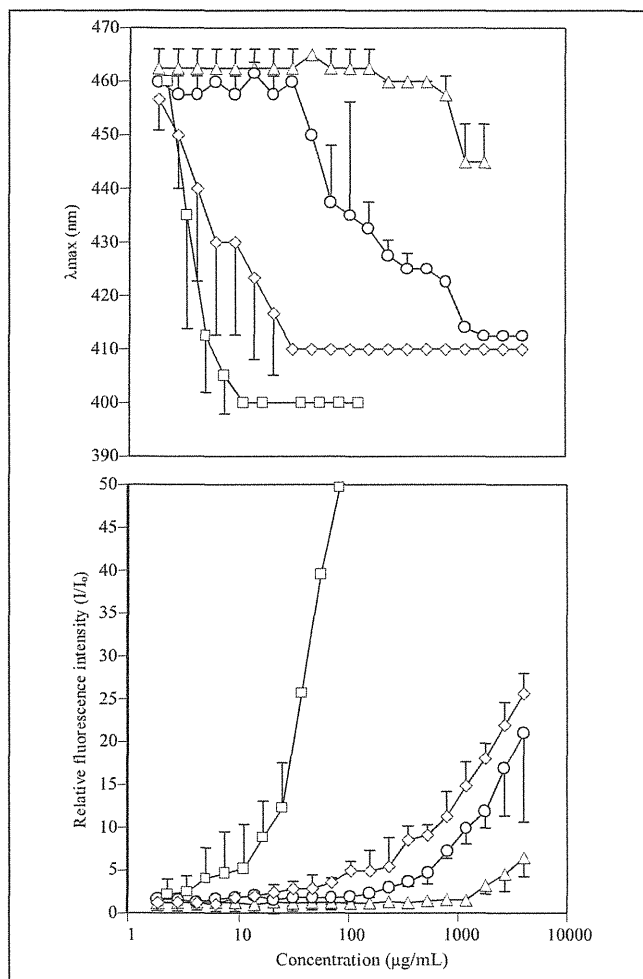**Figure 1** - Preparation of the styrene maleic acid copolymer.

Figure 2 - Emission maximum (λ max) and relative fluorescence intensity of PNA as a function of the logarithm of the concentration of SMA (1 k) (O), But-SMA (1 k) ($\triangle$), SMA (7 k) ($\Diamond$), and SMA (10 k) ($\square$). Each point represents the mean of 4 to 5 measurements.

aggregation concentration (CAC) of the self-assembled nanoparticles formed was determined by fluorescence probe techniques using N-phenyl-1-naphthylamine (PNA). PNA, which is strongly hydrophobic, has an extremely low solubility in water and preferentially dissolves into the hydrophobic core of micelles.

The relative fluorescence intensity increased with increasing concentration of each SMA, as shown in *Figure 2*. The relative fluorescence intensity versus concentration curve for each SMA showed a sharp increase from which the CAC values were estimated. The CAC was determined from the intersection point of two straight lines: one line drawn through the points at the lowest polymer concentrations and another line through the points along the rapidly rising part of the plot. The CAC of each SMA largely depended on the molecular weight of the SMA; the highest cohesive force was observed with the 10 kDa SMA (*Table I*). Furthermore, the shift in the emission maximum of the PNA to a lower wavelength, a so-called blue shift, was a function of the concentration of each SMA (*Figure 2*). The blue shift is observed when the PNA molecule moves from an aqueous environment to a hydrophobic environment [22, 27, 28].

2. Toxicity assay of SMAs

Amphiphilic SMAs behave like surfactants, which generally induce cytotoxicity. *Figure 3a* shows the hemolytic activity of SMAs with
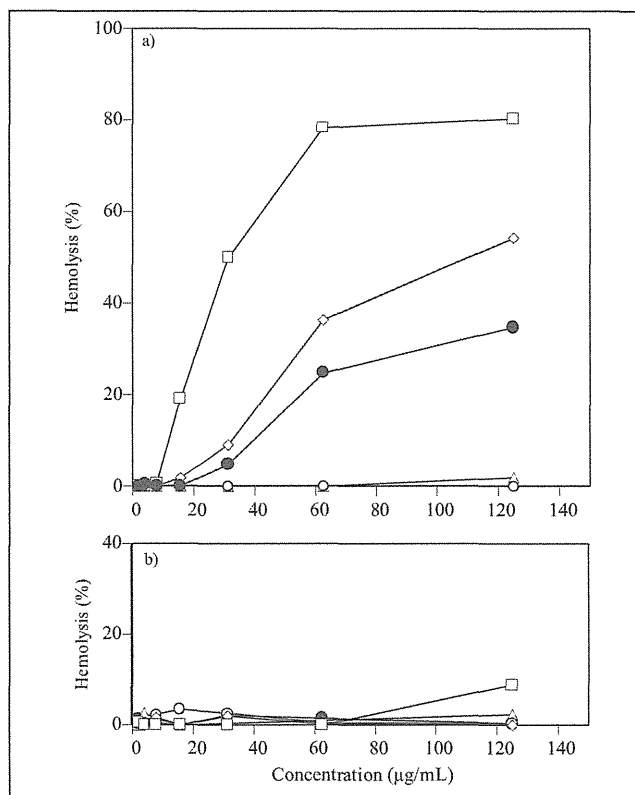

Figure 3 - Hemolysis of (a) mouse red blood cells and (b) sheep red blood cells in SMAs: SMA (1 k) (O), But-SMA (1 k) ($\triangle$), SMA (7 k) ($\Diamond$), SMA (10 k) ($\square$), and sodium deoxycholate (●).

Table I - Properties of SMA nanoparticles.

Samples	CAC (μg/mL)	AmB-loaded particle			ATRA-loaded particle		
		AmB loading (w/w%)	Particle size (nm)	Zeta potential (mV)	ATRA loading (w/w%)	Particle size (nm)	Zeta potential (mV)
But-SMA (1 k)	600	10.9	27.4 ± 1.7	- 40.0 ± 1.6	-	-	-
SMA (1 k)	110	10.6	21.4 ± 1.6	- 36.6 ± 4.3	-	-	-
SMA (7 k)	100	11.7	6.2 ± 0.5	- 41.4 ± 3.7	10.1	9.1 ± 1.1	- 42.8 ± 1.1
SMA (10 k)	20	14.6	6.8 ± 0.2	- 42.6 ± 2.3	10.7	7.7 ± 0.8	- 36.7 ± 1.2

J. DRUG DEL. SCI. TECH., 23 (3) 231-237 2013

Styrene maleic acid anhydride copolymer (SMA) for the encapsulation of sparingly water-soluble drugs in nanoparticles
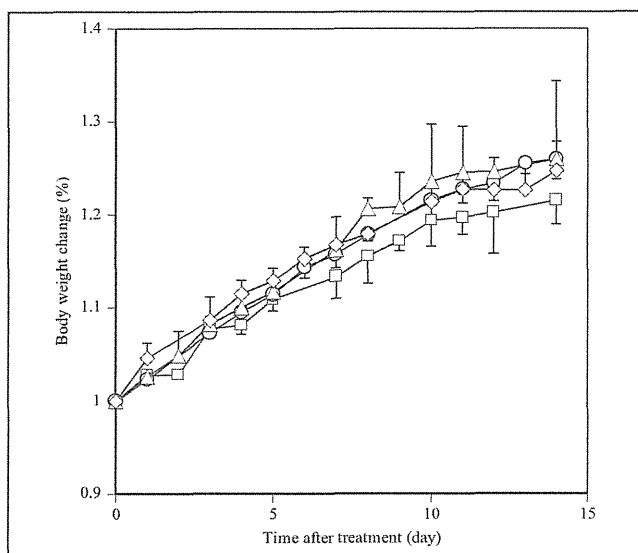*S. Yamamoto, Y. Kaneo, H. Maeda*

Figure 4 - Changes in the body weight of mice treated with SMA (1 k) (O), But-SMA (1 k) (Δ), SMA (7 k) (◊), or 5 % glucose (□). SMAs were injected intravenously as a single dose of 20 mg/kg at day 0. Values given are the mean ± SD for groups of 4-5 mice.
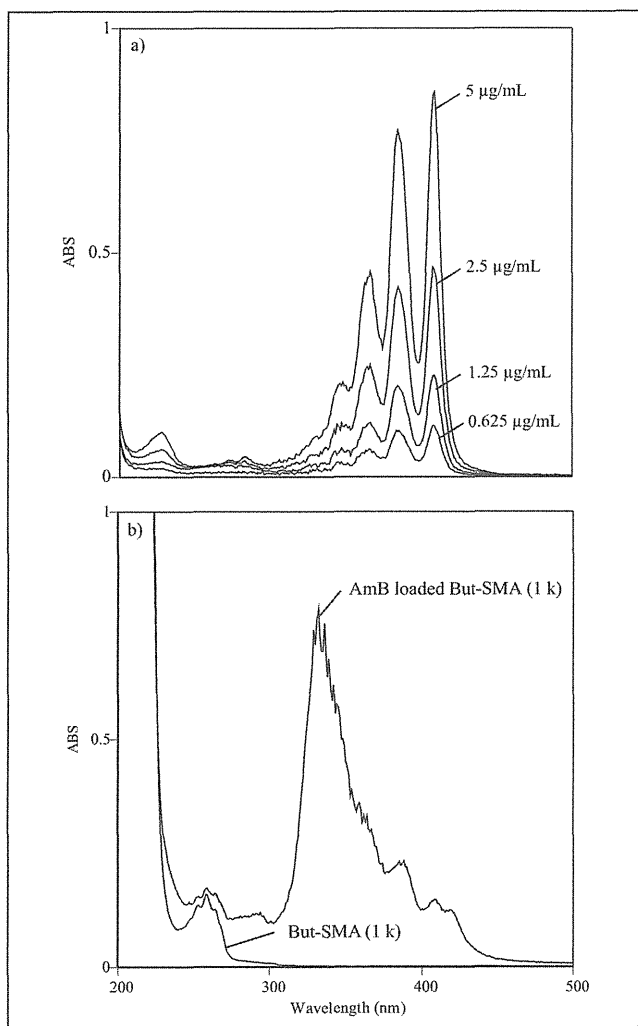

Figure 5 - (a) UV absorption of AmB in 50 % methanol solution at 5, 2.5, 1.25, and 0.625 μg/mL. (b) UV absorption of AmB loaded But-SMA (1 k) and But-SMA (1 k) at 250 μg/mL.

different molecular weights toward mouse RBCs. SMA (10 k) caused 50 % hemolysis above 30 μg/mL, whereas SMA (7 k) caused 50 % hemolysis above 110 μg/mL. In contrast, But-SMA (1 k) and SMA (1 k) were completely non-hemolytic up to 120 μg/mL. The positive control desoxycholate, which is frequently used as a micellation compound for many insoluble drugs, actually showed 50 % hemolysis at 300 μg/mL. On the other hand, the sheep RBCs showed a different tendency (*Figure 3b*). SMAs with the same concentrations induced no hemolysis in the sheep RBCs. A species difference between mouse and sheep was observed in the hemolysis experiments (*Figure 3*).

Because body weight loss is a sensitive and objective sign of physiological issues, the changes in the body weights of the mice were examined. Mice were treated with But-SMA (1 k), SMA (1 k), or SMA (7 k) at 20 mg/kg. A 5 % glucose solution was used as a control. As shown in *Figure 4*, no body weight loss was observed in mice treated with the SMAs. The higher molecular weight SMA (7 k) demonstrated hemolysis, but the response was almost same as that of the desoxycholate. As shown in *Figure 4*, we found no significant differences in body weight between mice treated with SMAs and mice treated with 5 % glucose. Therefore, SMA is expected to be a safe compound.

3. Drug loading to SMA nanoparticles

The loading of drugs into the nanoparticles occurred instantaneously when a small amount of DMSO containing the drug was added to SMA in water. The data on AmB loading (w/w %) in SMA nanoparticles is listed in *Table 1*. The loading efficiencies of SMAs range between 10.6 and 14.6 w/w %, depending on the molecular weight of the vehicle, whereas the loading efficiency of ATRA was approximately 10 w/w %. Free AmB is sparingly soluble in water, whereas both the Fungizone and the AmB-loaded SMA nanoparticles yielded a clear solution. The SMA also clearly rendered ATRA soluble.

The size of AmB-loaded nanoparticles varied from 6.2 to 27.4 nm, whereas the size of ATRA loaded nanoparticles varied from 7.7 to 9.1 nm, as determined by DLS. All the drug-loaded nanoparticles had a negative charge of approximately -40 mV (*Table 1*).

UV spectroscopy was used to investigate the aggregation state of AmB associated with the nanoparticles. The UV absorbance spectrum of AmB in 50 v/v % methanol, representing the monomeric form, showed high-intensity peaks at 405, 384, and 366 nm and a low-intensity peak at 348 nm (*Figure 5a*) [29]. The absorbance spectrum of AmB-loaded SMA showed a broad peak with high intensity at 331 nm and peaks of lower intensity at 405, 384, and 366 nm, demonstrating that AmB was in an aggregated state (*Figure 5b*) [24, 30]. AmB in the SMA nanoparticles aggregated in a manner similar to the desoxycholate micelle preparation Fungizone [31, 32].

The UV absorbance spectrum of ATRA in 50 v/v % methanol showed a high-intensity peak at 340 nm (*Figure 6a*). *Figure 6b* indicates that SMA effectively encapsulated ATRA into the nanoparticles.

The properties of the SMA nanoparticles were investigated using HPSEC with a differential refractometer. *Figure 7* shows the chromatograms of the But-SMA (1 k), SMA (1 k), SMA (7 k), and SMA (10 k). All the SMA nanoparticle entities were eluted near the exclusion volume of the column. This result indicates that the SMA molecules formed rigid nanoparticles. HPSEC results agree with the results of the CAC determination using PNA (*Figure 2*). Therefore, we proposed encapsulating drugs in the hydrophobic inner core of the nanoparticles. This approach was supported by the absorbance spectrum of the AmB-loaded SMA, which exhibited a broad, intense peak at 331 nm, demonstrating that AmB is in a self-aggregated state (*Figure 5*).

Furthermore, the drug-loaded SMA nanoparticles were also eluted near the exclusion volume of the column (*Figure 8*). Elution peaks were also detected using a photodiode array detector. The peak retention time for AmB-loaded But-SMA (1 k) was 5.8 min for each detection
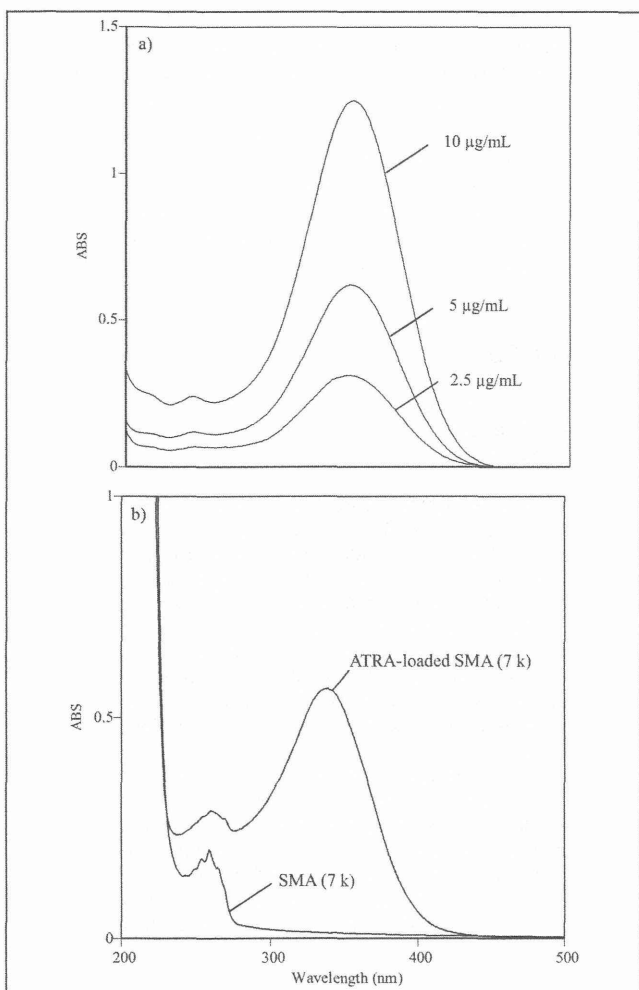
Styrene maleic acid anhydride copolymer (SMA) for the encapsulation
of sparingly water-soluble drugs in nanoparticles
S. Yamamoto, Y. Kaneo, H. Maeda

J. DRUG DEL. SCI. TECH., 23 (3) 231-237 2013

Figure 6 - (a) UV absorption of ATRA in 50 % methanol solution at 10,
5, and 2.5 μg/mL. (b) UV absorption of ATRA loaded SMA (7 k) at 50 μg/
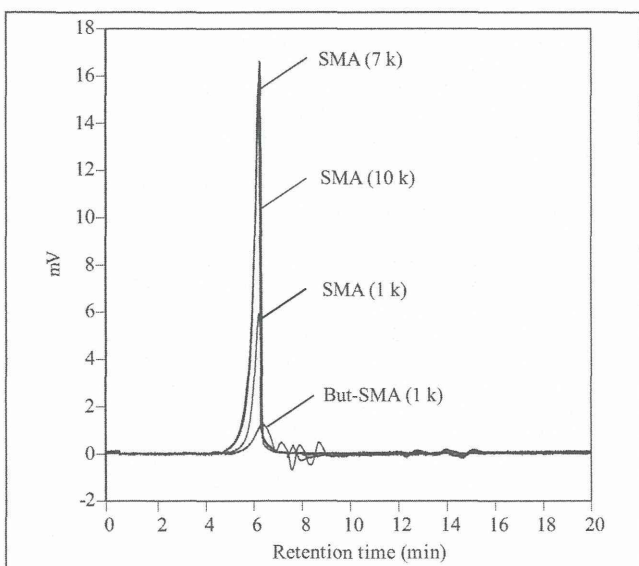mL and SMA at 250 μg/mL.

Figure 7 - HPSEC chromatograms of SMA (1 k), But-SMA (1 k), SMA
(7 k), and SMA (10 k). HPSEC was carried out on an HPLC system
equipped with a differential refractometer. A 7.8 × 300 nm, TSKgel
G4000PWXL column was used at 40 °C. The mobile phase was water,
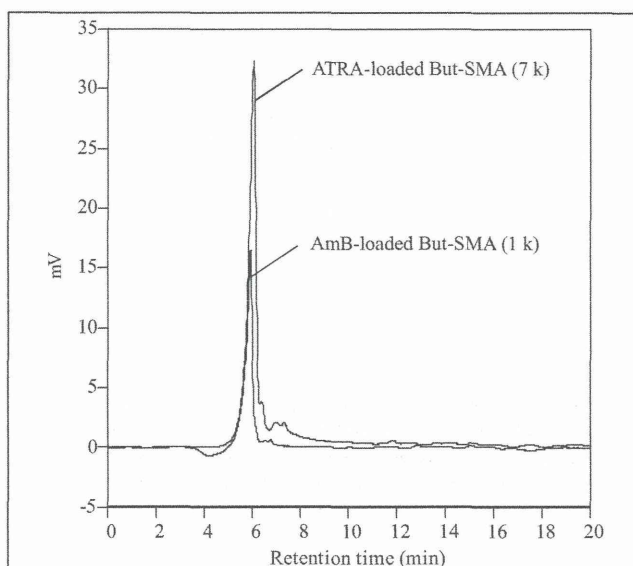and the flow rate was 1.0 mL/min.

Figure 8 - HPSEC chromatograms of AmB-loaded But-SMA (1 k) and
ATRA-loaded SMA (7 k). HPSEC was carried out on an HPLC system
equipped with a differential refractometer. A 7.8 × 300 nm, TSKgel
G4000PWXL column was used at 40 °C. The mobile phase was water,
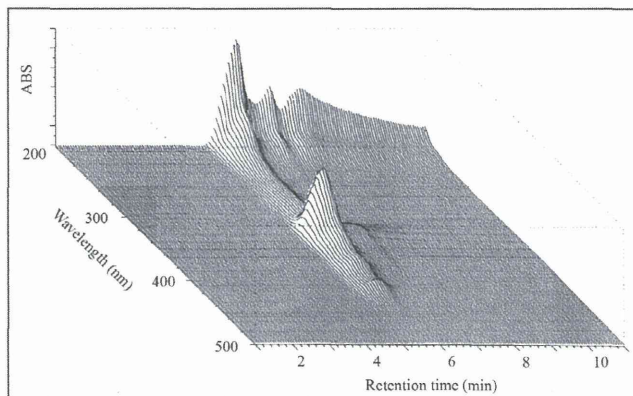and the flow rate was 1.0 mL/min.

Figure 9 - Three-dimensional chromatogram of AmB-loaded But-SMA.
The peak retention time for the AmB-loaded But-SMA (1 k) was 5.8 min
for the 405, 380, 360, and 335 nm cross sections. High-performance
size-exclusion chromatography was carried out using an HPLC system
equipped with a photodiode array detector. A 7.8 × 300 mm, TSKgel
G4000PWXL column was used at 40 °C. The mobile phase was water,
and the flow rate was 1.0 mL/min.

wavelength (405, 380, 360, and 335 nm), as observed in *Figure 9*. These
results indicated that the introduction of hydrophobic drugs into the
core of the nanoparticle makes the nanoparticle more rigid and more
stable. This tendency was especially prominent in the AmB-loaded
But-SMA (1 k) nanoparticles, which is evident when comparing the
HPSEC chromatograms of But-SMA and AmB-loaded But-SMA in
Figures 7 and 8.

4. Biodistribution of drug-loaded SMA nanoparticles

Figure 10 shows the tissue distribution of the AmB loaded into
But-SMA (1 k) and Fungizone particles at various times after intrave-
nous injection in mice. But-SMA (1 k) nanoparticles produced plasma
levels of AmB that were similar to, but slightly higher than, those of
Fungizone. However, it was found that the concentration of AmB in
the liver after the injection of the AmB-loaded SMA nanoparticles
was significantly lower than that of the Fungizone micelles (p < 0.05).
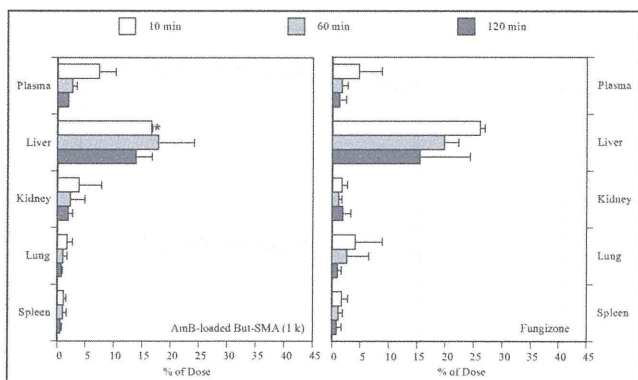We also examined the biodistributions of AmB-loaded SMA (1 k) and

J. DRUG DEL. SCI. TECH., 23 (3) 231-237 2013

Styrene maleic acid anhydride copolymer (SMA) for the encapsulation
of sparingly water-soluble drugs in nanoparticles
S. Yamamoto, Y. Kaneo, H. Maeda

Figure 10 - AmB levels in the blood and tissues after a single injection of AmB-loaded But-SMA (1 k) nanoparticles or Fungizone at an equivalent dose of 2 mg/kg in mice. Values given are the mean ± SD for groups of 4-5 mice. *p < 0.05: significant difference versus Fungizone.
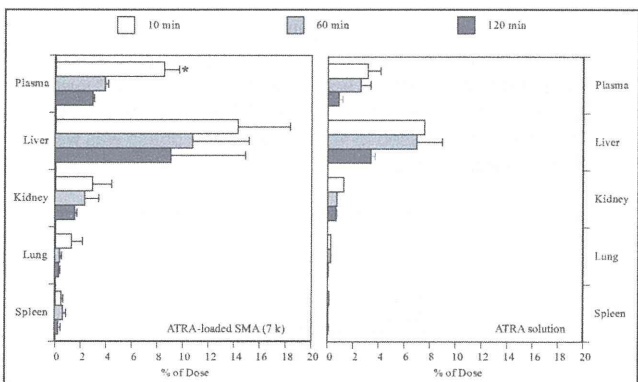

Figure 11 - ATRA levels in the blood and tissues after a single injection of ATRA-loaded SMA (7 k) or ATRA solution at an equivalent dose of 2 mg/kg in mice. Values given are the mean ± SD for groups of 4-5 mice. *p < 0.01: significant difference versus ATRA solution.

AmB-loaded SMA (7 k) (data not shown), which were similar to that of AmB-loaded But-SMA (1 k).

Figure 11 shows the tissue distribution of the ATRA-loaded SMA (7 k) and ATRA solution. ATRA-loaded SMA (7 k) was adopted to examine *in vivo* distribution, because SMA (7 k) was less hemolytic than SMA (10 k) in mice as shown in *Figure 3a*. The ATRA solution was prepared for intravenous injection by dissolving ATRA in 0.9 % NaCl-0.3 % NaOH (w/v) solution according to a previously described procedure [15, 33]. ATRA-loaded SMA nanoparticles showed significantly higher ATRA plasma levels than the ATRA solution (p < 0.01). However, the same tendency was observed for ATRA levels in the tissue distribution (*Figure 11*).

The AmB or ATRA plasma concentration (10 % of dose) was equal to 30 μg/mL of SMA in mice after administration of AmB (2 mg/kg) or ATRA (2 mg/kg) as a SMA nanoparticle (*Figures 10 and 11*). AmB is intravenously administered as Fungizone at a dose of 0.125-0.25 mg/kg, whereas ATRA (Vesanoid) is orally administered at a dose of 20-25 mg (15 mg/m²) in clinical treatment. The concentrations of SMAs (7 k or 10 k) to solubilize and carry the clinical dose of these drugs were then estimated to be much lower than the concentrations which induce the hemolysis, as shown in *Figure 3a*.

*

SMA is a useful material for medical applications demonstrated through the success of SMANCS. In this study, we investigated the biological safety and the functions of nanoparticle formations with

varying molecular weights of SMA. Only by simple hydrolysis of SMA without further chemical modification, amphiphilic carrier molecules could be obtained. We have prepared AmB-loaded SMA and ATRA-loaded SMA nanoparticles for the first time; these are self-assembled nanoparticles with a high drug loading capacity. Encapsulation in SMA nanoparticles could effectively increase the overall water solubility of these sparingly water-soluble drugs. Furthermore, a relatively high retention of AmB and ATRA in the blood circulation was also demonstrated in an *in vivo* animal experiment. Amphiphilic SMAs can give AmB and ATRA new pharmaceutical capabilities.

REFERENCES

1. Winek C.L., Burgun J.J. - Acute and subacute toxicology and safety evaluation of SMA 1440-H resin. - Clin. Toxicol., **10**, 255-260, 1977.
2. Maeda H., Bharate G.Y., Daruwalla J. - Polymeric drugs for efficient tumor-targeted drug delivery based on EPR-effect. - Eur. J. Pharm. Biopharm., **71**, 409-419, 2009.
3. Fang J., Nakamura H., Maeda H. - The EPR effect: unique features of tumor blood vessels for drug delivery, factors involved, and limitations and augmentation of the effect. - Adv. Drug. Deliv. Rev., **63**, 136-151, 2011.
4. Daruwalla J., Greish K., Malcontenti-Wilson C., Muralidharan V., Iyer A., Maeda H., Christophi C. - Styrene maleic acid-pirarubicin disrupts tumor microcirculation and enhances the permeability of colorectal liver metastases. - J. Vasc. Res., **46**, 218-228, 2009.
5. Daruwalla J., Nikfarjam M., Greish K., Malcontenti-Wilson C., Muralidharan V., Christophi C., Maeda H. - *In vitro* and *in vivo* evaluation of tumor targeting styrene-maleic acid copolymer-pirarubicin micelles: survival improvement and inhibition of liver metastases. - Cancer Sci., **101**, 1866-1874, 2010.
6. Nakamura H., Fang J., Gahininath B., Tsukigawa K., Maeda H. - Intracellular uptake and behavior of two types zinc protoporphyrin (ZnPP) micelles, SMA-ZnPP and PEG-ZnPP as anticancer agents; unique intracellular disintegration of SMA micelles. - J. Control. Release, **155**, 367-375, 2011.
7. Fang J., Greish K., Qin H., Liao L., Nakamura H., Takeya M., Maeda H. - HSP32 (HO-1) inhibitor, copoly(styrene-maleic acid)-zinc protoporphyrin IX, a water-soluble micelle as anticancer agent: *in vitro* and *in vivo* anticancer effect. - Eur. J. Pharm. Biopharm., **81**, 540-547, 2012.
8. Gallis H.A., Drew R.H., Pickard W.W. - Amphotericin B: 30 years of clinical experience. - Rev. Infect. Dis., **12**, 308-329, 1990.
9. Brajtburg J., Bolard J. - Carrier effects on biological activity of amphotericin B. - Clin. Microbiol. Rev., **9**, 512-531, 1996.
10. Deray G. - Amphotericin B nephrotoxicity. - J. Antimicrob. Chemother., **49**, Suppl. 1, 37-41, 2002.
11. Laniado-Laborin R., Cabrales-Vargas M.N. - Amphotericin B: side effects and toxicity. - Rev. Iberoam. Micol., **26**, 223-227, 2009.
12. Guo L.S. - Amphotericin B colloidal dispersion: an improved antifungal therapy. - Adv. Drug Deliv. Rev., **47**, 149-163, 2001.
13. Tomii Y. - Lipid formulation as a drug carrier for drug delivery. - Curr. Pharm. Des., **8**, 467-474, 2002.
14. Herbrecht R., Natarajan-Ame S., Nivoix Y., Letscher-Bru V. - The lipid formulations of amphotericin B. - Expert Opin. Pharmacother., **4**, 1277-1287, 2003.
15. Shelley R.S., Jun H.W., Price J.C., Cadwallader D.E. - Blood level studies of all-trans- and 13-cis-retinoic acids in rats using different formulations. - J. Pharm. Sci., **71**, 904-907, 1982.
16. Kwon G.S. - Polymeric micelles for delivery of poorly water-soluble compounds. - Crit. Rev. Ther. Drug Carrier Syst., **20**, 357-403, 2003.
17. Thassu D., Pathak Y., Deleers M. - Nanoparticlate drug delivery systems: an overview. - In: Nanoparticulate Drug Delivery Systems, D. Thassu, M. Deleers, Y.V. Pathak (Eds)., CRC Press, 2007, p. 1-31.
18. Yallapu M.M., Reddy M.K., Labhasetwar V. - Nanogels: chemistry

to drug delivery. - In: Biomedical Applications of Nanotechnology, V. Labhasetwar., D.L. Leslie-Pelecky (Eds.), John Wiley & Sons, 2007, p. 131-171.

19. Fahr A., Liu X. - Drug delivery strategies for poorly water-soluble drugs. - Expert Opin. Drug Deliv., **4**, 403-416, 2007.

20. Greish K., Sawa T., Fang J., Akaike T., Maeda H. - SMA-doxorubicin, a new polymeric micellar drug for effective targeting to solid tumours. - J. Control. Release, **97**, 219-230, 2004.

21. Greish K., Nagamitsu A., Fang J., Maeda H. - Copoly(styrene-maleic acid)-pirarubicin micelles: high tumor-targeting efficiency with little toxicity. - Bioconjug. Chem., **16**, 230-236, 2005.

22. Akiyoshi K., Deguchi S., Moriguchi N., Yamaguchi S., Sunamoto J. - Self-aggregates of hydrophobized polysaccharides in water. formation and characteristics of nanoparticles. - Macromolecules, **26**, 3062-3068, 1993.

23. Lavasanifar A., Samuel J., Kwon G. S. - Micelles self-assembled from poly(ethylene oxide)-block-poly(N-hexyl stearate L-aspartamide) by a solvent evaporation method: effect on the solubilization and haemolytic activity of amphotericin B. - J. Control. Release, **77**, 155-160, 2001.

24. Charvalos E., Tzatzarakis M.N., Van Bambeke F., Tulkens P.M., Tsatsakis A.M., Tzanakakis G.N., Mingeot-Leclercq M.P. - Water-soluble amphotericin B-polyvinylpyrrolidone complexes with maintained antifungal activity against *Candida* spp. and *Aspergillus* spp. and reduced haemolytic and cytotoxic effects. - J. Antimicrob. Chemother., **57**, 236-244, 2006.

25. Golas C.L., Prober C.G., MacLeod S.M., Soldin S.J. - Measurement of amphotericin B in serum or plasma by high-performance liquid chromatography. - J. Chromatogr., **278**, 387-395, 1983.

26. Li Y., Qi X.R., Maitani Y., Nagai T. - PEG-PLA diblock copolymer micelle-like nanoparticles as all-trans-retinoic acid carrier: *in vitro* and *in vivo* characterizations. - Nanotechnology, **20**, 055106, 2009.

27. Brito R.M., Vaz W.L. - Determination of the critical micelle concentration of surfactants using the fluorescent probe N-phenyl-1-naphthylamine. - Anal. Biochem., **152**, 250-255, 1986.

28. Jung S.W., Jeong Y.I., Kim S.H. - Characterization of hydrophobized pullulan with various hydrophobicities. - Int. J. Pharm., **254**, 109-121, 2003.

29. Oda T., Maeda H. - Binding to and internalization by cultured cells of neocarzinostatin and enhancement of its actions by conjugation with lipophilic styrene-maleic acid copolymer. - Cancer Res., **47**, 3206-3211, 1987.

30. Barwicz J., Christian S., Gruda I. - Effects of the aggregation state of amphotericin B on its toxicity to mice. - Antimicrob. Agents Chemother., **36**, 2310-2315, 1992.

31. Tiyaboonchai W., Limpeanchob N. - Formulation and characterization of amphotericin B-chitosan-dextran sulfate nanoparticles. - Int. J. Pharm., **329**, 142-149, 2007.

32. Adams M.L., Kwon G.S. - Relative aggregation state and hemolytic activity of amphotericin B encapsulated by poly(ethylene oxide)-block-poly(N-hexyl-L-aspartamide)-acyl conjugate micelles: effects of acyl chain length. - J. Control. Release, **87**, 23-32, 2003.

33. Su J., Zhang N., Ho P.C. - Evaluation of the pharmacokinetics of all-trans-retinoic acid (ATRA) in Wistar rats after intravenous administration of ATRA loaded into tributyrin submicron emulsion and its cellular activity on caco-2 and HepG2 cell lines. - J. Pharm. Sci., **97**, 2844-2853, 2008.

ACKNOWLEDGMENTS

MANUSCRIPT

Review Article

The link between infection and cancer: Tumor vasculature, free radicals, and drug delivery to tumors via the EPR effect

Hiroshi Maeda[1]

Institute of Drug Delivery System Research, Sojo University, Kumamoto, Japan

This review focuses primarily on my own research, including pathogenic mechanisms of microbial infection, vascular permeability in infection and tumors, and effects of nitric oxide (NO), superoxide anion radical (O_2^-), and 8-nitroguanosine in the enhanced permeability and retention (EPR) effect for the tumor-selective delivery of macromolecular agents (nanomedicines). Infection-induced vascular permeability is mediated by activation of the kinin-generating protease cascade (kallikrein–kinin) triggered by exogenous microbial proteases. A similar mechanism operates in cancer tissues and in carcinomatosis of the pleural and peritoneal cavities. Infection also stimulates O_2^- generation via activation of xanthine oxidase while generating NO by inducing NO synthase. These chemicals function in mutation and carcinogenesis and promote inflammation, in which peroxynitrite (a product of O_2^- and NO) activates MMP, damages DNA and RNA, and regenerates 8-nitroguanosine and 8-oxoguanosine. We showed vascular permeability by using macromolecular drugs, which are not simply extravasated through the vascular wall into the tumor interstitium but remain there for prolonged periods. We thus discovered the EPR effect, which led to the rational development of tumor-selective delivery of polymer conjugates, micellar and liposomal drugs, and genes. Our styrene–maleic acid copolymer conjugated with neocarzinostatin was the first agent of its kind used to treat hepatoma. The EPR effect occurs not only because of defective vascular architecture but also through the generation of various vascular mediators such as kinin, NO, and vascular endothelial growth factor. Although most solid tumors, including human tumors, show the EPR effect, heterogeneity of tumor tissue may impede drug delivery. This review describes the barriers and countermeasures for improved drug delivery to tumors by using nanomedicines. (*Cancer Sci* 2013; 104: 779–789)

As the recipient of the Tomizo Yoshida Award of the Japanese Cancer Association in 2011, I herein describe my personal recollections of my research. This review covers the pathogenic mechanisms of microbial infection and generation of endogenous bradykinin (also called kinin) and free radicals O_2^- and NO in bacterial and viral infections. This review also discusses selective delivery of anticancer macromolecular agents (now called nanomedicines) to tumor tissue, which take advantage of the vascular permeability of tumor tissue (analogous to inflamed tissue). Projects involving the antitumor antibiotic protein neocarzinostatin (NCS, 13 kDa) were pursued in my laboratory at the Department of Microbiology, Kumamoto University School of Medicine (Kumamoto, Japan) for more than two decades,[1–3] and this research led me to the field of nanomedicine.

Around 1978, my research focused on developing an antitumor agent that would target metastatic tumors, or more specifically, to target to the lymphatic system. For this purpose, I had to design an anticancer agent with lipophilic and macromolecular characteristics, because these features would favor preferential recovery of the agent through the lymphatic system from lymphatic networks in the interstitial space after extravasation from blood vessel lumina. In 1978, therefore, I prepared a conjugate of NCS with SMA, in which SMA conferred lipophilic and polymeric characteristics.[1–3] This agent was the first polymer-conjugated macromolecular anticancer drug, named SMANCS, and was reported as the first macromolecular anticancer agent having antimetastatic activity.[4–8] SMANCS possessed many advantages including lipid formulation using Lipiodol®,[9] as described later, and also effective to the multidrug resistance of tumor cells.[8–11]

Thereafter, we carried out more detailed pharmacological studies of SMANCS and other macromolecular drugs, including plasma proteins and synthetic polymers, which led to the discovery of the unique pharmacokinetics of polymeric drugs and, more importantly, the EPR effect.[5–8,12–15] We then investigated the EPR effect in greater detail and found that many vascular mediators, such as bradykinin (also called kinin), NO, $ONOO^-$, prostaglandins, vascular endothelial growth factor, collagenase, and more recently, carbon monoxide, are responsible for this effect (Table 1).[15–22] Our earlier studies of the kinin-generating cascade triggered by microbial proteases and biological generation of free radicals in infection were quite useful for understanding these vascular mediators and the EPR effect and for developing methods to further augment cancer drug delivery based on the EPR effect. The ultimate outcome of these studies can provide theoretical mechanism, and extend to the application of nanomedicines for tumor selective delivery to treat cancer in the future.

Relation of vascular permeability to infection and cancer: Inflammatory mediators in bacterial infection and cancer

We first discovered that kinin, the most potent pain-inducing endogenous peptide hormone, was generated by exogenous bacterial proteases through the activation of one or more steps in the kinin-generating cascade, which begins with stimulation of Hageman factor, or factor XII (which would lead to the blood coagulation cascade), and continues to involve prekallikrein to kallikrein (Fig. 1), and then generation of kinin from

---

Mediators†	Responsible enzymes and mechanisms‡	References
Bradykinin	Kallikrein/protease	16,19,32,33
NO	iNOS	17,18,96
VPF/VEGF	Involved in NO generation	76,77
Prostaglandins	Cyclooxygenase-1	76,77,95
Collagenase (proMMPs → MMP)	Activated from proMMPs by peroxynitrite or proteases	20
Peroxynitrite (ONOO⁻)	$NO + O_2^- \rightarrow ONOO^- \rightarrow proMMP \rightarrow MMP$	20
Carbon monoxide	Heme oxygenase-1	97
Induced hypertension	Using angiotensin II	70,77,89
Inflammatory cells and H_2O_2	Neutrophil/NADPH oxidase, etc.	
Transforming growth factor-β inhibitor		114
Vascular endothelial cell growth factor (VEGF)	Also involves NO	77,93
Tumor necrosis factor-α		115
Anticancer agents		
Heat		116

†Extensive production of vascular mediators that facilitate extravasation from normal and tumor vessels. ‡Enzymes or mechanisms involved in each process (see text for details). iNOS, inducible form of nitric oxide synthase; NO, nitric oxide; VEGF, vascular endothelial growth factor; VPF, vascular permeability factor.
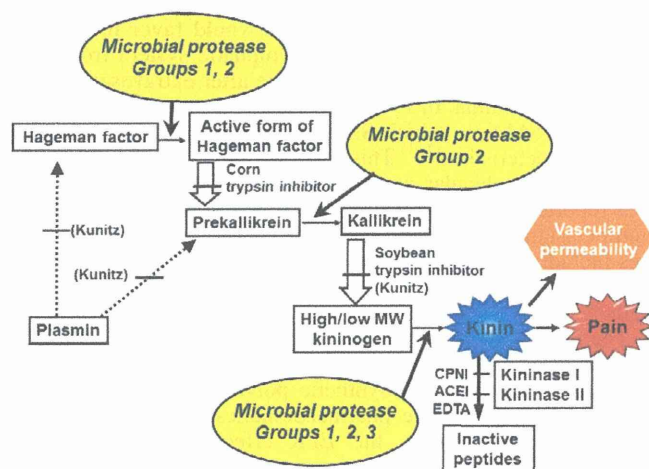

Fig. 1. Kinin-generating cascade activated by proteases, which begins with activation of Hageman factor (factor XII), continues to prekallikrein and kallikrein, then yields kinin (blue). Kinin stimulates vascular leakage (permeability). Tumor tissue has a more active cascade, which thus produces excessive kinin. Corn trypsin inhibitor, soybean trypsin inhibitor, and carboxypeptidase N inhibitor (CPNI) can inhibit this cascade. ACEI, angiotensin-converting-enzyme inhibitor; MW, molecular weight.

high- and low-molecular-weight kininogen in blood plasma. All pathogenic bacterial and fungal infections induce inflammation,[23–25] in which extravasation of plasma proteins is a hallmark event and causes edema and in which bradykinin is a key mediator. Similar such events were later found to occur in solid tumors. We have discovered no effective inhibitor in the body against all microbial proteases, including fungal protease, that we tested.[26–31]

With regard to cancer, we found a significantly high concentration of kinin, which was generated by the above-mentioned mechanism, in blood plasma and in peritoneal or pleural carcinomatosis in tumor-bearing hosts including humans.[32–34] Kinin generation was effectively inhibited by inhibitors of kallikrein such as soybean trypsin inhibiter or by kinin antagonists.[32–34]

Various tumor cells highly express bradykinin receptors, which lead to growth stimulation, angiogenesis, metastasis, and release of MMPs involving NO, prostaglandins, and various other cytokine signaling pathways.[35–38] We focused our attention, however, on vascular permeability in tumors and delivery of macromolecular drugs that was given i.v., which led to discovery of the EPR effect.

Wu and others in our department showed that the kinin antagonist HOE 140 (Hoechst, Frankfurt, Germany) or kallikrein inhibitors, such as soybean trypsin inhibitor, can block this extravasation of plasma proteins in cancer tissue.[19,20] Soybean trypsin inhibitor and other serine protease inhibitors (such as PMSF) effectively suppressed formation of peritoneal and pleural ascites,[32–34] in which the kinin concentration was quite high, and facilitated fluid accumulation.[16,32,33] Kinin antagonists were later found to suppress tumor growth, thus they may be good therapeutic targets in cancer therapy and pain control.[37,38] However, the involvement of bradykinin in tumor biology and pathogenesis warrants further investigation.

My experiences with protein anticancer drugs, that is, NCS and SMANCS, therefore made me realize, in the early 1980s, the potential use of the enhanced vascular permeability of solid tumors for delivery of macromolecular anticancer drugs.[36–38]

Endogenous free radical generation in infection: A significant cause of tissue damage by O_2^- and mutation

We focused on two research areas of infectious diseases: one was exogenous bacterial proteases, which involve the kinin cascade and degenerative tissue damage; and the other was biological free radicals, that is, ROS and RNS, as derived from NO. We first found that O_2^- was generated in excess during respiratory infection with influenza virus in mice.[39,40] Our initial hypothesis, that Nox of infiltrated leukocytes would play a major role, was determined to be untrue. Instead, the major source of O_2^- generation was excessive activation of XO to about 400-fold from xanthine dehydrogenase. This enzyme is involved in the latter part of adenosine catabolism: adenosine → inosine → hypoxanthine → xanthine → uric acid + $2 \times O_2^-$; in this cascade, adenosine deaminase activity increased approximately 170-fold,[39–42] and Nox was second in importance.

Our discovery of excessive generation of O_2^- in viral infection was an unprecedented finding that was proved by means of three completely different methods. The first used pyran copolymer-conjugated SOD, which removed O_2^- and markedly improved the survival rate (Fig. 2a). The polymer–SOD conjugate was designed to have a plasma half-life more than 100 times longer than that of native SOD, which is cleared from
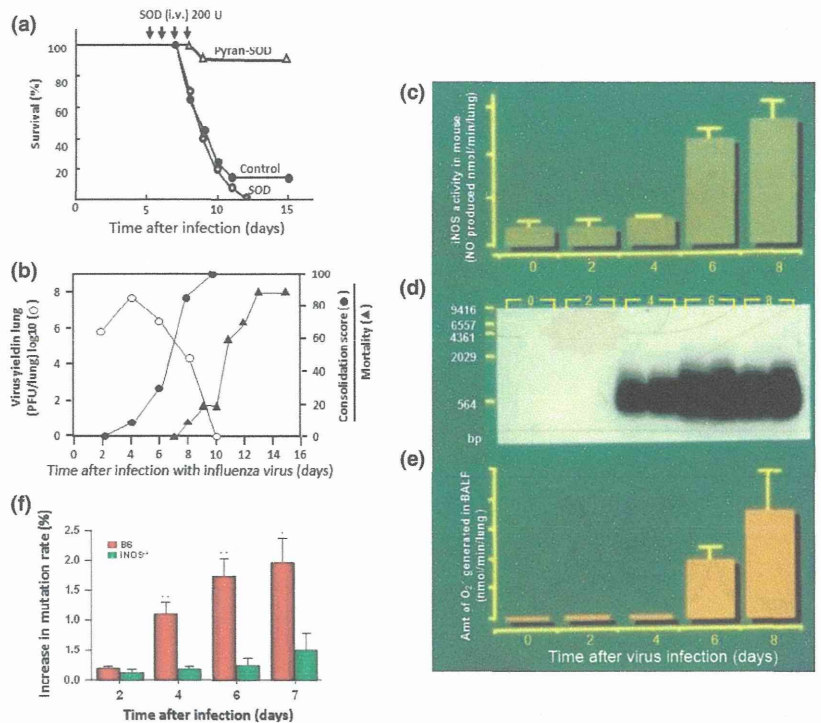
Fig. 2. Pathological and molecular events in influenza virus-infected mice. (a) Treatment of influenza virus-infected mice with native superoxide dismutase (SOD) (○), polymer (pyran)-conjugated SOD (△), or no drug (control) (●). (b) Time course of virus yield (○), consolidation score (●), and mortality (▲). All these events occurred separately. (c–e) Activity of the inducible form of nitric oxide synthase (iNOS) and superoxide (O_2^-). (c) iNOS activity. (d) Induction of PCR-detectable iNOS mRNA. (e) Amount of O_2^- generated after virus infection. (f) Effect of mutant virus formation in wild-type iNOS$^+$ B6 mice (red bars) and iNOS$^{-/-}$ B6 transgenic mice (green bars). More mutant virus was formed in NO-generating wild-type mice, which indicated a need for NO for viral mutation. BALF, bronchoalveolar lavage fluid.

the blood circulation in mice within a few minutes.[39,40] This conjugate was likely the first polymer-conjugated therapeutic enzyme, the idea for which derived from our experience with SMANCS, as described in more detail later.

The second method used the XO inhibitor allopurinol, which improved the survival rate of virus infected mice in a dose-dependent manner. The third was injection of adenosine, which generates inosine and then hypoxanthine (a substrate of XO) and O_2^-, which itself facilitated a pathogenic effect and resulted in severe exacerbation of this viral infection and an accelerated death rate of mice.[39–41]

During influenza virus infection, the amount of virus (i.e. virus yield), consolidation score of the lung, and mortality rate of infected mice increased, but not simultaneously. Figure 2(b) illustrates that the amount of virus in the alveolar compartment, as determined by bronchoalveolar lavage, was highest on day 4 after infection then decreased to undetectable levels on day 10, whereas pathological manifestations as indicated by the consolidation score and O_2^- generation started to increase on day 6 and reached a maximum on day 10, when the mice started to die and virus was no longer detectable.[39–41] Thus, all three events occurred separately, not simultaneously, and I coined the phrase "virus disease in the absence of virus," for situations in which the amount of virus did not completely correspond to pathological severity.[42]

As another important finding, the data showed that oxygen radicals (ROS) can be generated by a truly biological event as a host response *in vivo*, not just by intense UV irradiation, X-ray, or γ-ray exposure *in vitro*. That the generation of free radicals is clearly an etiological principle in infectious diseases can also be stated. In other words, this pathological mechanism extends beyond the boundary of Robert Koch's postulate or paradigm.[42] This mechanism will also offer alternative therapeutic options against infectious diseases by using scavengers of O_2^- (Fig. 2a) or by inhibiting ROS-generating systems that will reduce the pathogenic potential and cure diseases.

We subsequently found that another biological free radical, NO, is excessively generated under conditions similar to those of influenza virus infection (Fig. 2c–e), which also possesses a pathogenic potential.[43–48] That O_2^- and NO react rapidly and form ONOO$^-$, which is an agent with extremely potent oxidizing and nitrating activities occurring simultaneously, is well known. ONOO$^-$ would therefore modify DNA and RNA by nitration or oxidation, or by strand breaks (Fig. 2f).[43–50] This increased mutation by ROS and RNS was also shown in bacteria[49,50] as well as influenza and Sendai viruses,[44,47,48] and antioxidant scavengers suppressed mutagenesis and carcinogenesis.[49–52] These data support the idea that carcinogenesis induced by infection and inflammation would proceed through free radical generation or oxidative stress.[51,52]

Furthermore, a finding relevant to free radical-induced carcinogenesis is that 8-nitroguanosine becomes a substrate for NOS. Also, the NADPH reductase, cytochrome b5 reductase, and reductase domain of NOS similarly generate O_2^- (Fig. 3a).[53–57] In separate but related studies, we showed that various heterocyclic amines (all 11 kinds) and NCS effectively produced O_2^-. All these chemicals are mutagens in the presence of NADPH and cytochrome P450 reductase (Fig. 3b).[53–56] Also, the mutation rate of *Salmonella typhimurium* (Ames strains) paralleled to the amount of O_2^- produced.[57]

We collaborated with Dr. Tatematsu of Aichi Cancer Center Research Institute (Nagoya, Japan) in studies of our novel phenolic antioxidant compound named canolol, which suppressed *Helicobacter pylori*-induced inflammation, ONOO$^-$ cytotoxicity, and carcinogenic potential, whereas canolol did not affect the number (colony-forming units) of *H. pylori* bacilli.[49–51] These data support the proposal that free radical generation is a key process in the mediation of inflammation and chemical carcinogenesis, as previously expected.[52] Additional details about the chemical damage to nucleic acids by ONOO$^-$ have been provided by Niles *et al.*,[58] Sawa and Ohshima,[59] and others.

In view of the relation among inflammation, oxidative damage, and carcinogenesis, Okada, Kobayashi, Tanaka, Cao, Shimizu, Muto, Surh, and many others showed the potent